

Article

## Estimating Biomass of Barley Using Crop Surface Models (CSMs) Derived from UAV-Based RGB Imaging

Juliane Bendig <sup>1,\*</sup>, Andreas Bolten <sup>1</sup>, Simon Bennertz <sup>1</sup>, Janis Broscheit <sup>1</sup>, Silas Eichfuss <sup>1</sup> and Georg Bareth <sup>1,2</sup>

<sup>1</sup> Institute of Geography, GIS & RS, University of Cologne, 50923 Cologne, Germany; E-Mails: andreas.bolten@uni-koeln.de (A.B.); s.bennertz@googlemail.com (S.B.); janis.b@arcor.de (J.B.); silas.eichfuss@googlemail.com (S.E.); g.bareth@uni-koeln.de (G.B.)

<sup>2</sup> ICASD-International Center for Agro-Informatics and Sustainable Development, College of Resources and Environmental Sciences, China Agricultural University, Beijing 100193, China

\* Author to whom correspondence should be addressed; E-Mail: juliane.bendig@uni-koeln.de; Tel.: +49-221-470-6551; Fax: +49-221-470-4917.

External Editors: Clement Atzberger and Prasad S. Thenkabail

Received: 16 July 2014; in revised form: 20 October 2014 / Accepted: 21 October 2014 /

Published: 28 October 2014

---

**Abstract:** Crop monitoring is important in precision agriculture. Estimating above-ground biomass helps to monitor crop vitality and to predict yield. In this study, we estimated fresh and dry biomass on a summer barley test site with 18 cultivars and two nitrogen (N)-treatments using the plant height (PH) from crop surface models (CSMs). The super-high resolution, multi-temporal (1 cm/pixel) CSMs were derived from red, green, blue (RGB) images captured from a small unmanned aerial vehicle (UAV). Comparison with PH reference measurements yielded an  $R^2$  of 0.92. The test site with different cultivars and treatments was monitored during “Biologische Bundesanstalt, Bundessortenamt und Chemische Industrie” (BBCH) Stages 24–89. A high correlation was found between PH from CSMs and fresh biomass ( $R^2 = 0.81$ ) and dry biomass ( $R^2 = 0.82$ ). Five models for above-ground fresh and dry biomass estimation were tested by cross-validation. Modelling biomass between different N-treatments for fresh biomass produced the best results ( $R^2 = 0.71$ ). The main limitation was the influence of lodging cultivars in the later growth stages, producing irregular plant heights. The method has potential for future application by non-professionals, *i.e.*, farmers.

**Keywords:** UAV; optical; remote sensing; RGB; 3D; biomass estimation; crop surface model; plant height; summer barley; precision agriculture

---

## 1. Introduction

Monitoring crops throughout the vegetation period is one prerequisite for precision agriculture [1,2]. In addition to natural factors, like water availability or soil quality, knowledge about the health status, nutrient supply and effects of agricultural management practices helps when estimating the predicted yield of a field [3–5]. Such knowledge can be obtained from crop parameters, such as plant height (PH), biomass, plant nitrogen content, soil nitrogen content and LAI, amongst other variables [6,7]. Biomass plays an important role in yield prediction and for management optimization. For the latter, the nitrogen nutrition index (NNI), the ratio of measured and critical nitrogen (N) content, is commonly used as a tool for determining the ideal amount of N needed to maximize yield while preventing over-fertilization [8,9]. The relationship between biomass and N concentration is used in the N dilution curve, from which the critical N content is derived [9,10]. Hence, biomass is a crucial parameter for calculating the NNI.

The NNI input values can be measured either destructively or non-destructively by remote sensing. Biomass can be estimated through spectral reflectance measurements [11] from space [12,13], from the air [14–16] or from the ground [7,17–19]. However, these measurements often involve sophisticated and expensive equipment that needs careful calibration. Alternatively, PH is also positively correlated with crop biomass [20]. In combination with a non-vegetation ground model, PH can be obtained by quantifying the height of a canopy using crop surface models (CSMs) [21–23]. The suitability of terrestrial laser scanning (TLS) for biomass estimation is demonstrated by Tilly *et al.* [24,25] for paddy rice and for sugar beet by Hoffmeister *et al.* [26]. A good correlation between PH and grain yield in barley, oat and wheat is given by Lumme *et al.* [27] and by Ehlert *et al.* [28] in oilseed rape, winter rye, winter wheat and grassland. Besides laser scanning approaches, 3D geometry information from an unmanned aerial vehicle (UAV), in combination with a high-resolution digital camera, is used for CSM generation. UAVs, sometimes referred to as remotely-piloted aerial systems (RPAS) or unmanned aerial systems (UAS), are the emerging tools to be used for small-scale remote sensing [17,29,30]. A few studies exist for biomass estimation, e.g., [31,32], using UAV-based near-infrared imaging. Comparisons of UAVs with airborne platforms (for larger areas) and TLS show competitive results [25,27]. In an agricultural context, UAVs have been used, for example, for crop status analysis using near-infrared or thermal data [33–35] or crop mapping. This study uses UAV-based data from a small-scale summer barley field experiment to evaluate how successfully CSMs can predict biomass.

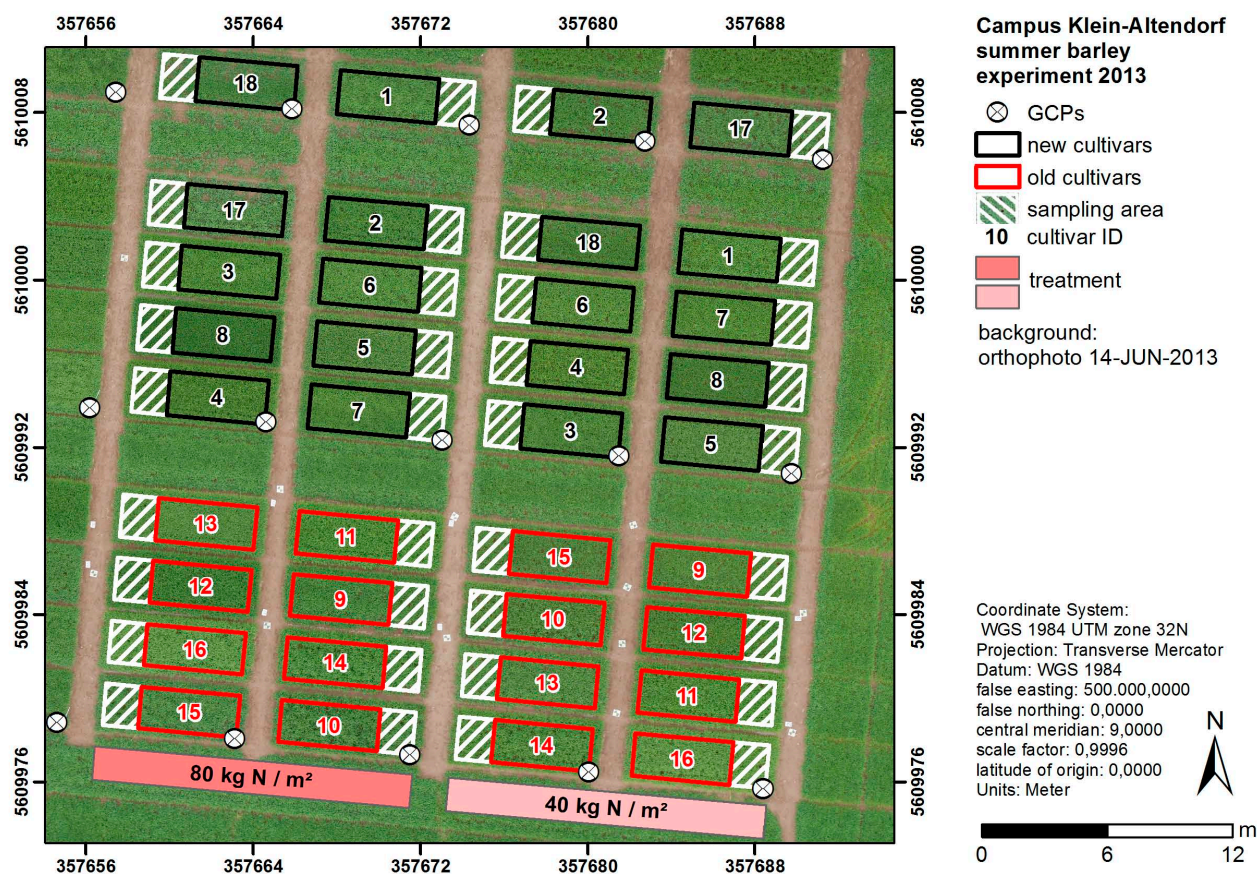
## 2. Materials and Methods

### 2.1. Test Site: Campus Klein-Altendorf, 2013

The study site is located at the Campus Klein-Altendorf agricultural research station (50°37'N, 6°59'E, altitude 186 m), 40 km south of Cologne, Germany. The summer barley experiment consists of

18 barley cultivars, of which ten are new cultivars and eight are old cultivars (Figure 1). They were randomized over 54 plots with a size of  $3 \times 7$ -m, a  $300$ -plants/ $m^2$  seeding density and a  $0.104$ -m row spacing. The plots were fertilized with either  $40$  or  $80$  kg N/ha. Each plot was divided into a  $3 \times 5$ -m measuring area and a  $3 \times 2$ -m sampling area. Destructive biomass sampling was carried out for two replicas ( $40$  and  $80$  kg N/ha) of each variety (number of samples ( $n$ ) =  $36$ ). Additionally, the reference plant height ( $PH_{ref}$ ) was measured manually in each plot ( $n$  =  $10$ ). Ground control points (GCPs) were distributed evenly across the field, making them easily identifiable in the images. The GCPs were made of  $0.3 \times 0.3$ -m laminated card board, which was attached to wooden poles that were fixed in the ground. We then measured the position with a differential global positioning system (DGPS, HiPer<sup>®</sup> Pro Topcon, Tokyo, Japan) with  $0.01$ -m horizontal and vertical precision.

**Figure 1.** Test site: summer barley experiment at Campus Klein-Altendorf agricultural research station in 2013. GCPs, ground control points used for crop surface model (CSM) generation.



## 2.2. Biomass Sampling

Destructive above-ground biomass sampling of  $0.04$   $m^2$  was carried out within the sampling areas of each plot (Figure 1). The roots were clipped, samples were cleaned and stem, leaves and ears were weighed separately on the same day for fresh biomass measurement. For obtaining dry biomass, the samples were then dried at  $70$  °C for  $120$  h, and each plant organ was weighed again separately. The

values were rescaled to kg per m<sup>2</sup>. The sampling took place either on the same day or on the day before or after the UAV flights (Table 1). The biomass sampling area was excluded from the CSM calculation.

**Table 1.** Details of unmanned aerial vehicle (UAV) flight campaigns (CSM resolution 0.01 m) and destructive biomass sampling.

Type	Date	Number of Images Collected	BBCH <sup>*1</sup>	Point Density (pt./m <sup>2</sup> )	Ø Image Overlap <sup>*2</sup>
UAV (ground model)	30 April 2013	216			
UAV	14 May 2013	378		2878	>9
Biomass	14 May 2013		tillering (21–27)		
UAV	28 May 2013	783		2675	>9
Biomass	28 May 2013		tillering-stem elongation (25–35)		
UAV	14 June 2013	363		2958	>9
Biomass	12 June 2013		booting (41–47)		
UAV	25 June 2013	300		3452	>9
Biomass	25 June 2013		inflorescence emergence, heading (51–59)		
UAV	8 July 2013	342		2836	>9
Biomass	9 July 2013		development of fruit (71–75)		
UAV	23 July 2013	265		2653	>9
Biomass	22 July 2013		development of fruit-ripening (77–89)		

<sup>\*1</sup> “Biologische Bundesanstalt, Bundessortenamt und Chemische Industrie” (BBCH); <sup>\*2</sup> the number of images covering the same part of the area of interest (AOI).

### 2.3. Platform

In this study, we used the multi-rotor MK-Oktokopter developed by HiSystems (see [21] for details). The payload capacity is 1 kg. The flight duration varies between 5–15 min, depending on the batteries and payload chosen. The red, green, blue (RGB) optical sensor was mounted on a gimbal that maintained a near nadir camera position. The gimbal position is adjusted to the pitch and roll movement that is measured by the onboard gyroscopes of the airframe [21,36]. During the flight, position, altitude and flying speed were automatically logged to a memory card. The MK-tool autopilot was used to set the flight waypoints.

### 2.4. Sensor

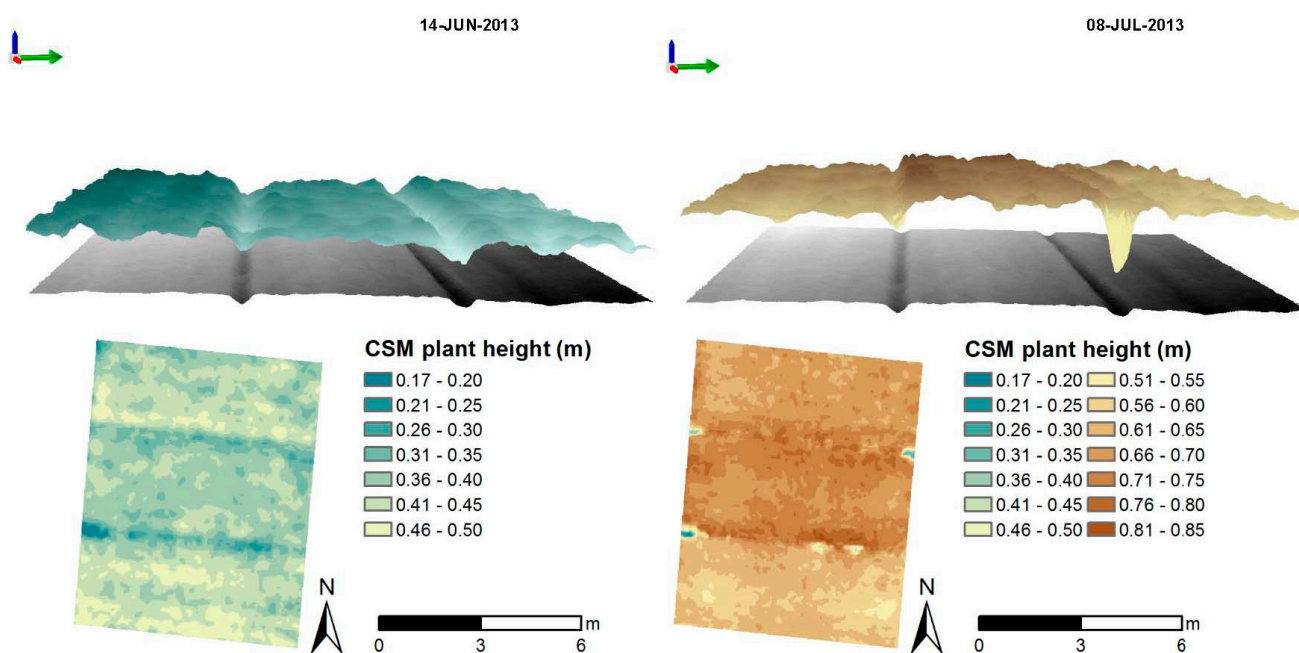
RGB imagery was collected with a Panasonic Lumix GX1 digital camera (16 Megapixels, 4608 × 3464, with a Lumix G 20 mm (F1.7 aspheric (ASPH)) fixed lens). The angular field of view is 55.8° horizontal × 38.9° vertical, resulting in 0.009-m ground sampling distance (GSD) at 50 m above ground level. A cable connects the camera to the flight control of the MK-Oktokopter, which enables

triggering via the remote control. The camera is set to continuous data capture at 2 frames per second (fps) with fixed aperture and exposure according to the light conditions and saves images to a secure digital (SD) memory card.

### 2.5. Generating CSMs

Generating crop surface models requires (a) mosaicking of the collected images, (b) point cloud generation, and (c) digital surface model (DSM) export. Here, the DSM represents the crop surface and is referred to as CSM hereafter. It has to be subtracted from a ground model (Table 1, Figure 2) in order to obtain (d) the PH. For Steps a–c, we use Agisoft PhotoScan Professional, a structure from motion (SfM) [37] software that performs a bundle adjustment based on matching features between the images. The result is a 3D reconstruction of the geometry that enables export of a CSM, in our case, a 0.01-m resolution \*TIF-file (Figure 2; [38,39]). For enhanced absolute spatial accuracy, the GCPs were imported into PhotoScan prior to (b), where they were projected to all images automatically after being placed in a single image [40]. We then manually verified and adjusted the positions if necessary. Finally, the CSM is exported in \*TIF-image format.

**Figure 2.** CSM over ground model (**top**) and derived plant height (**bottom**) of Plots 8, 7 and 1 (from left to right) of the eastern row of the test site for 14 June and 8 July 2013.



Further processing was carried out in Esri ArcGIS® 10.2.1. The CSM was clipped with the 36 plots, which form the area of interest (AOI). To account for boundary effects, the plots were reduced by 0.3 m on each end, and the areas where destructive biomass sampling was performed were excluded. In the next step, the CSM is subtracted from the ground model to obtain the PH. The mean PH was calculated for each plot (Figure 2, Table 2) and used for the biomass estimation with a regression model. This process is repeated for the CSM of each date. The workflow for deriving PH from CSMs is described in detail in [21]. An example of the ground model and the CSM for two sample dates is presented in Figure 2, as well as the derived PH.

**Table 2.** Descriptive statistics of CSM plant height ( $PH_{CSM}$ ), ground reference plant height ( $PH_{ref}$ ) (linear regression) and above-ground fresh and dry biomass (exponential regression) for all plots ( $n = 216$ ). SE = standard error;  $n$  = number of samples.

	$PH_{ref}$ (m)	$PH_{CSM}$ (m)	Fresh Biomass ( $kg/m^2$ )	Dry Biomass ( $kg/m^2$ )
Min	0.14	-0.03	0.22	0.03
Max	1.00	0.80	8.29	2.70
Mean	0.55	0.43	3.24	0.81
SE	0.25	0.25	1.96	0.68
n	216	216	216	216

## 2.6. Statistical Analyses

The correlation and regression analyses were carried out in Microsoft<sup>®</sup> Excel<sup>®</sup> 2013 and IBM<sup>®</sup> SPSS<sup>®</sup> Statistics 22.0.0.0. The mean PH per plot obtained from the CSM ( $PH_{CSM}$ ) was evaluated against the mean PH obtained from the reference ground measurements ( $PH_{ref}$ ). The result is presented in a scatter plot together with a linear regression equation.

For the biomass estimation, the multi-temporal dataset ( $n = 216$ ) was divided into five different calibration and validation datasets (Table 3). Exponential regression equations were derived for  $PH_{CSM}$  versus fresh biomass and  $PH_{CSM}$  versus dry biomass for the calibration datasets and evaluated by their coefficient of determination ( $R^2$ ). The resulting regression models from the calibration datasets were applied to the validation datasets and analyzed by linear correlation between observed biomass and predicted biomass. The results are compared based on the root mean square error (RMSE), relative error (RE in %) and standard error (SE), which equals the standard deviation (Table 4).

**Table 3.** Coefficients of determination ( $R^2$ ) for PH (CSM and ground reference, linear regression) and above-ground fresh and dry biomass (exponential regression) for all plots ( $n = 216$ ); lin. = linear, exp. = exponential;  $p < 0.0001$  for all  $R^2$ .

$R^2$	$PH_{ref}$ (m)	$PH_{CSM}$ (m)	Fresh Biomass ( $kg/m^2$ )	Dry Biomass ( $kg/m^2$ )
$PH_{ref}$ (m)	1			
$PH_{CSM}$ (m)	0.92 (lin.)	1		
fresh biomass ( $kg/m^2$ )	0.76 (exp.)	0.81 (exp.)	1	
dry biomass ( $kg/m^2$ )	0.79 (exp.)	0.82 (exp.)	0.67 (lin.)	1

## 3. Results

### 3.1. Plant Height and Biomass Samples

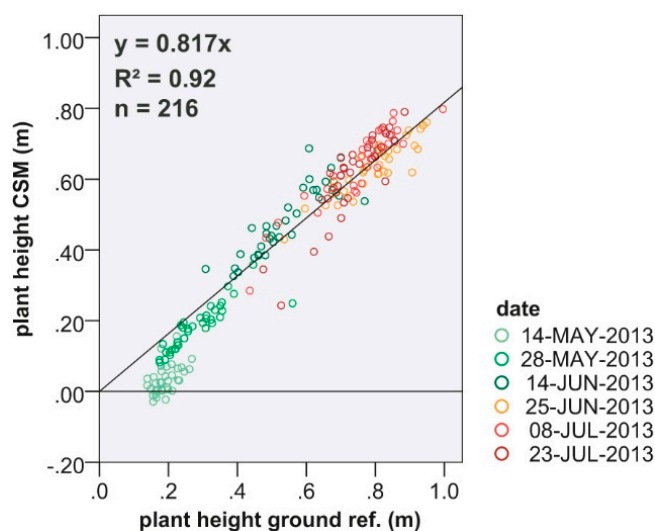
The test site was flown seven times between 30 April and 23 July 2013, at 50 m above ground level, of which the first dataset served as the non-vegetative ground model. Descriptions of the dataset are given in Table 1. Destructive biomass sampling was carried out for “Biologische Bundesanstalt, Bundessortenamt und Chemische Industrie” (BBCH) Stages 21–89 that equal the tillering until

ripening stage. From 25 June onwards, lodging occurred in the plots with four of the old cultivars (10, 11, 12 and 14 in Figure 1).

**Table 4.** Regression characteristics of observed *versus* predicted biomass. M1: 70% calibration, 30% validation; M2a: model for 40 kg N/m<sup>2</sup> applied on plots treated with 80 kg N/m<sup>2</sup>; M2b: model for 80 kg N/m<sup>2</sup> applied on plots treated with 40 kg N/m<sup>2</sup>; M3a: model for old cultivars applied on new cultivars; M3b: model of new cultivars applied on old cultivars. n = sample number of validation dataset; SE = standard error; R<sup>2</sup> = coefficient of determination; with p < 0.0001; RMSE = root mean square error; RE = relative error.

Calibration/Validation Dataset	Regression Model	n	SE (kg/m <sup>2</sup> )	R <sup>2</sup>	RMSE (kg/m <sup>2</sup> )	RE (%)
<b>Fresh Biomass</b>						
M1: 70%/30%	BIOM = 0.642 × exp(PH × 3.082)	66	3.21	0.71	1.95	60.87
M2a: 40/80 kg N/m <sup>2</sup>	BIOM = 0.534 × exp(PH × 3.411)	108	3.46	0.61	2.35	67.72
M2b: 80/40 kg N/m <sup>2</sup>	BIOM = 0.741 × exp(PH × 2.858)	108	2.97	0.71	1.60	54.04
M3a: old/new cultivars	BIOM = 0.690 × exp(PH × 3.080)	120	3.49	0.61	2.15	61.50
M3b: new/old cultivars	BIOM = 0.591 × exp(PH × 3.135)	96	2.87	0.72	1.77	61.79
<b>Dry Biomass</b>						
M1: 70%/30%	BIOM = 0.073 × exp(PH × 4.309)	66	0.77	0.60	0.59	76.50
M2a: 40/80 kg N/m <sup>2</sup>	BIOM = 0.057 × exp(PH × 4.922)	108	0.98	0.49	0.83	84.61
M2b: 80/40 kg N/m <sup>2</sup>	BIOM = 0.083 × exp(PH × 3.960)	108	0.61	0.61	0.42	68.41
M3a: old/new cultivars	BIOM = 0.081 × exp(PH × 4.242)	120	0.67	0.39	0.54	79.88
M3b: new/old cultivars	BIOM = 0.063 × exp(PH × 4.469)	96	0.83	0.68	0.64	76.28

**Figure 3.** Scatter plot for PH<sub>ref</sub> and PH<sub>CSM</sub> for all plots (n = 216). R<sup>2</sup> = coefficient of determination; p < 0.0001 for all R<sup>2</sup>.



We compared the PH derived from the CSM (PH<sub>CSM</sub>) to the reference measurements on the ground (PH<sub>ref</sub>) (Table 2, Figure 3). In general, PH<sub>CSM</sub> is about 0.1 m lower than PH<sub>ref</sub>, since the CSM represents the entire relief of the crop surface, not only the highest points of the plants (see the

Discussion). The coefficients of determination are classified hereafter as high ( $R^2 > 0.7$ ), medium ( $0.5 < R^2 < 0.7$ ) and low ( $R^2 < 0.5$ ). A high linear correlation of  $R^2 = 0.92$  is observed between  $PH_{CSM}$  and  $PH_{ref}$  (Figure 3). The overall standard errors (SEs) are similar for the  $PH_{CSM}$  and the  $PH_{ref}$  with 0.25 m.

The average fresh (and dry) biomass ranges between 0.2 and 8.3 (0.03 and 2.70)  $kg/m^2$  with an SE of 1.96 (0.68)  $kg/m^2$ . The exponential regression between  $PH_{CSM}$  and  $PH_{ref}$  and fresh biomass shows a high correlation of  $R^2 = 0.81$  and 0.76. The correlation is similar for dry biomass with an  $R^2$  of 0.82 and 0.79.

### 3.2. Biomass Modelling

#### 3.2.1. Model Development

In the first step, five exponential regression models between observed fresh and dry biomass and  $PH_{CSM}$  were developed and evaluated by their coefficients of determination ( $R^2$ ) (Figure 4). For Model 1 (M1), the data were split into a 70% calibration and 30% validation dataset by picking a randomized calibration dataset of 25 out of 36 samples for each date. For Models 2a and 2b, the data were split into a calibration dataset of 40  $kg N/m^2$  (M2a) and 80  $kg N/m^2$  (M2b). The calibration dataset for Model 3a (M3a) consists of the old cultivars, and for Model 3b (M3b), it consists of the new cultivars. M1 yielded an  $R^2$  of 0.79 for fresh biomass and 0.81 for dry biomass. M2a has a correlation of 0.84 for fresh biomass and 0.87 for dry biomass. For M2b, the correlation is 0.79 for fresh biomass and dry biomass. M3a produced an  $R^2$  of 0.78 for fresh and 0.73 for dry biomass and M3b 0.84 and 0.89. Note that all models are based on a different number of samples varying from 96 to 150 according to the experimental design. As we can see from Figure 4, the values tend to scatter increasingly for the later sampling dates.

#### 3.2.2. Model Application

In a second step, the derived regression models from the calibration datasets were applied to the validation datasets for all models (M1–M3b) (Figure 5). The correlation between observed biomass and predicted biomass is displayed in Table 4 and Figure 5. As we can see, the prediction of fresh biomass had the highest  $R^2$  values in the models, M3b (0.72), M2b (0.71) and M1 (0.70). The models M2a and M3a show medium correlations (0.61). In combination with the RMSE, RE and SE error measures, the model M2b performs best (RMSE = 1.6  $kg/m^2$ , RE = 54.04%, SE = 2.97). Model M2a fits worst with an RMSE of 2.35  $kg/m^2$ , an RE of 67.72% and an SE of 3.46  $kg/m^2$ . Again, the scattering of values increases with progressing vegetation stages. For the dry biomass, M3b, M2b and M1 show a medium  $R^2$  (0.68, 0.61 and 0.60), while the other models have a low correlation (0.49, 0.39). The regression characteristics show that M2b fits best to the biomass samples (RMSE = 0.42  $kg/m^2$ , RE = 68.41%, SE = 0.61), and M2a fits worst (RMSE = 0.83  $kg/m^2$ , RE = 84.61%, SE = 0.98  $kg/m^2$ ). The fit for the dry biomass models is 5 to 10% lower than that of the fresh models for each model.

**Figure 4.** Cross-validation relationship of fresh/dry biomass and CSM<sub>PH</sub> for calibration datasets. Model 1 (M1): 70%; M2a: 40 kg N/m<sup>2</sup>; M2b: 80 kg N/m<sup>2</sup>; M3a: old cultivars; M3b: new cultivars and all values; p < 0.0001 for all R<sup>2</sup>.

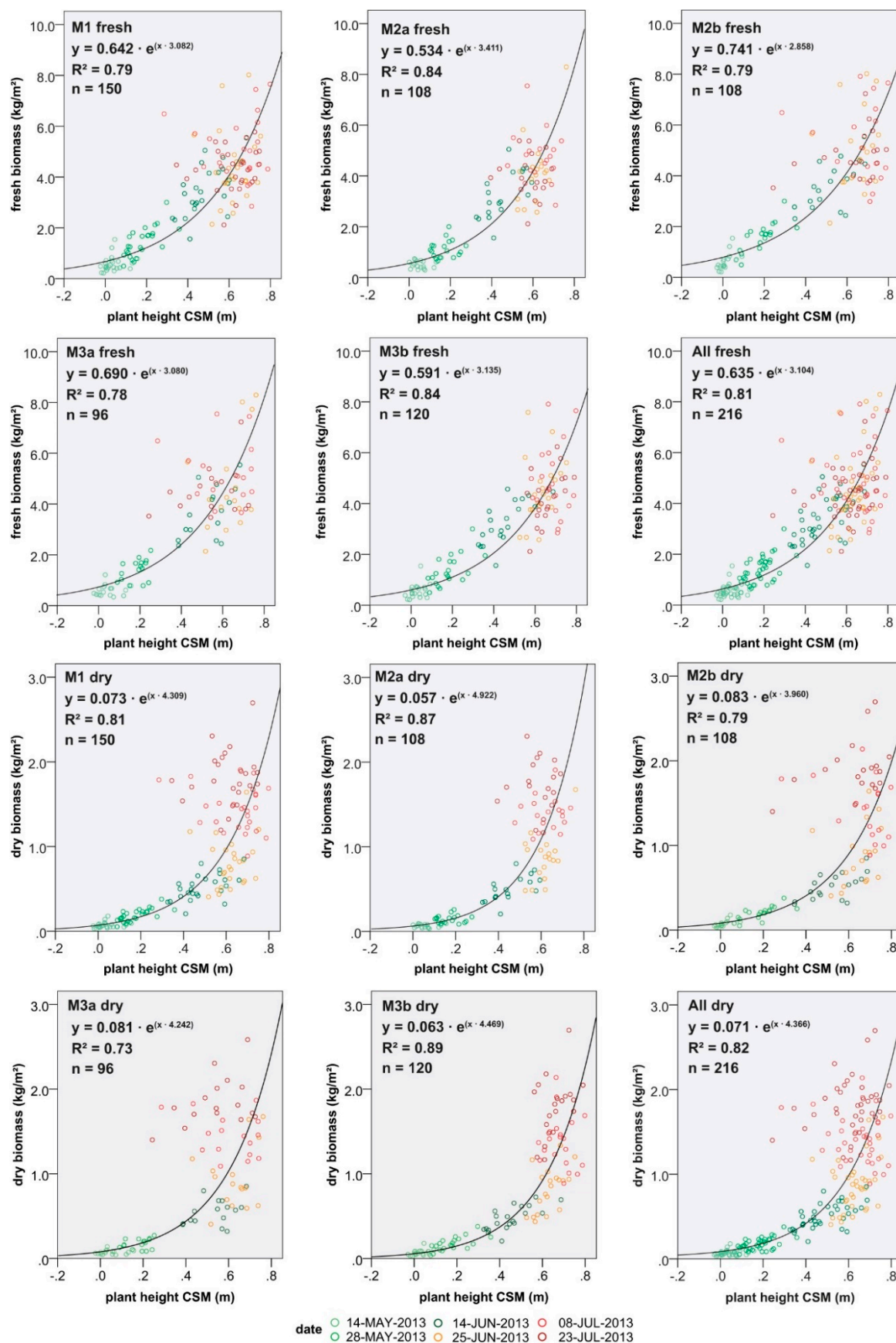
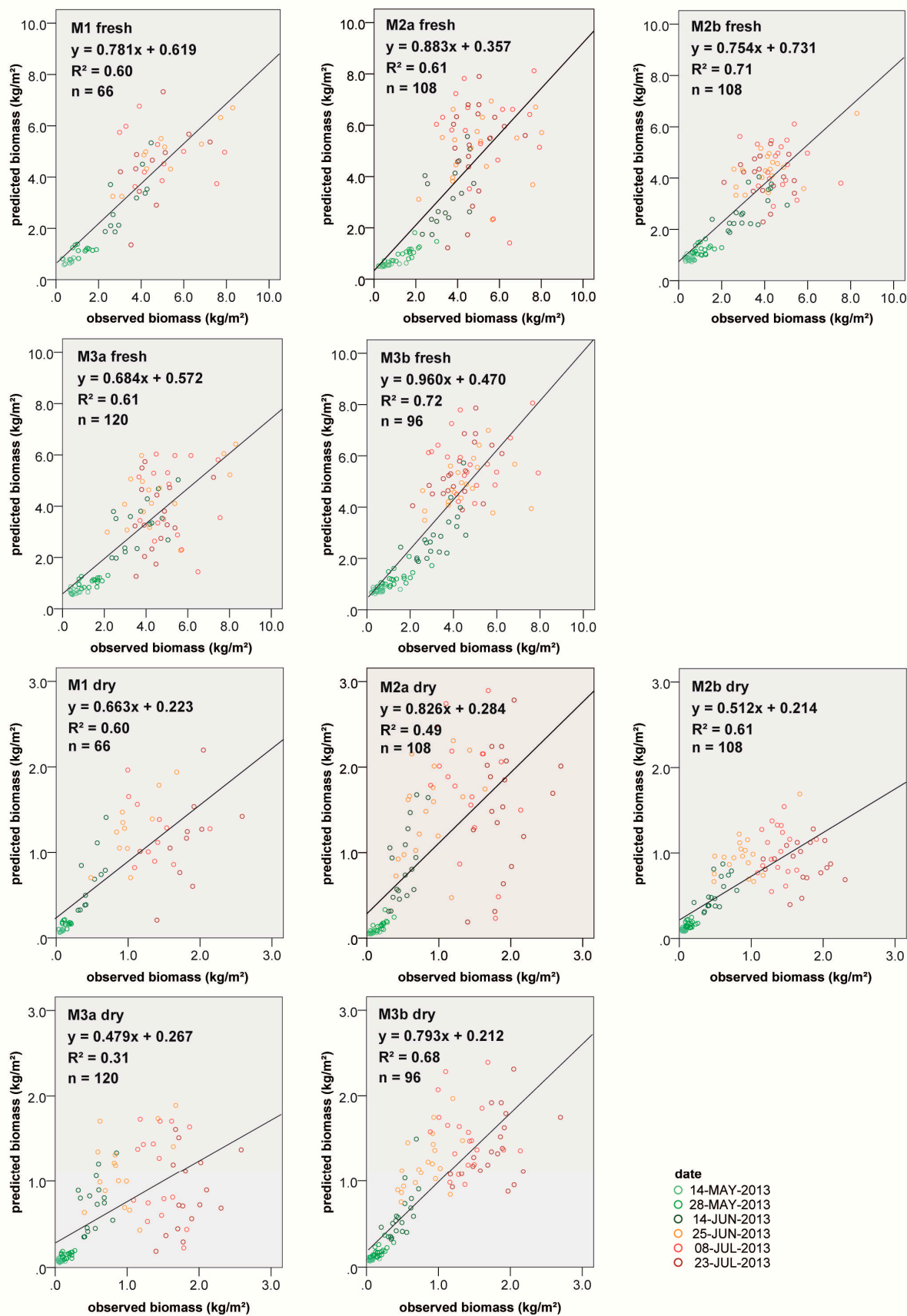


**Figure 5.** Cross-validation scatter plots for observed fresh and dry biomass *versus* predicted biomass derived from validation datasets M1–M3b (details in Table 4);  $p < 0.0001$  for all  $R^2$ .



#### 4. Discussion

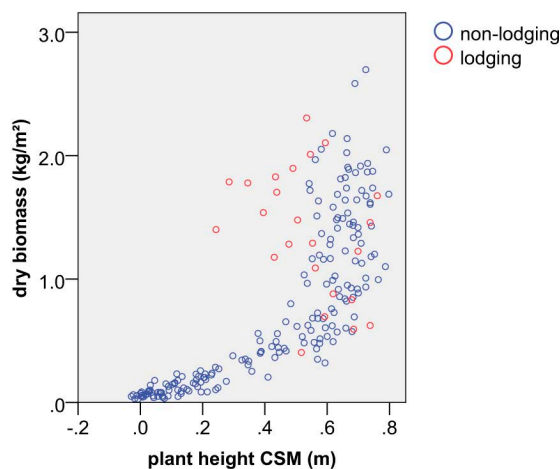
The CSM plant height ( $PH_{CSM}$ ) strongly correlates with the reference measurements ( $PH_{ref}$ ) ( $R^2 = 0.92$ ). For comparison, Ehlert *et al.* [41] achieved a coefficient of determination of 0.93–0.99 in oilseed rape, winter rye and winter wheat using a ground-based, non-destructive laser rangefinder. Busemeyer *et al.* [42] state an  $R^2$  of 0.97 in triticale using breed vision, a multi-sensor ground-based measuring platform consisting of a laser distance sensor, an ultrasonic sensor, a light curtain and a hyperspectral camera. However, ground-based methods can only be used in the accessible parts of a field and, thus, require interpolation [43].

In this study, the  $PH_{CSM}$  represents the mean plant height (PH) of all 0.01-m pixels in a plot. As a result, not only the top of the plant, for example the ears, is measured, but also the lower parts, like the leaves. Consequently, the detail of  $PH_{CSM}$  is higher than  $PH_{ref}$ , because  $PH_{CSM}$  contains more than one pixel per plant and, thus, not only the maximum height. In this context, the method for the PH reference measurements in the field should be discussed. Manual PH measurement is often subjective when the height is varying in a plot [44]. The results indicate that measuring 10 randomly chosen single plants does not produce a representative mean of the plot. To solve the problem, a transect could be measured every 0.05 m to better cover the canopy's heterogeneity. Another important factor is the influence of crop movement through wind. From our experience, wind primarily causes a shift in the x-y-direction and does not significantly influence PH measurements. The main constraint of the dataset is the lodging cultivars. A way to mitigate the effect of lodging can be to use the average maximum PH instead of the average mean PH. However, the objective of measuring PH by UAV-based imaging was satisfactorily reached.

CSMs allow spatial variation in PH, plant growth and, accordingly, biomass and yield to be identified. This ability is positive in comparison to point-wise sampling [2], where a high number of samples would be needed to allow for a comparable analysis. Even in small-scale field studies of <1 ha, the number of samples that can be collected in a manageable amount of time is limited. The number of samples might influence the comparison of point-wise biomass sampling and spatially measured CSM-derived biomass. In this study, the sampling area did not influence the model development, since it was separated from the measuring area.

The regression models for biomass estimation show that all models perform differently. The highest  $R^2$  occurs for fresh biomass in M3b ( $R^2$  0.72, RE 61.79%) and M2b ( $R^2$  0.71, RE 54.04%). The model quality for the dry biomass is generally lower, as is reflected in the high relative errors ranging between 68 and 85%. The models' main limiting factors are the four lodging cultivars, 10, 11, 12 and 14. Note that Cultivars 10, 11, 12 and 14 belong to the class of old cultivars. The scatter plot in Figure 6 shows the general exponential trend of the non-lodging plots (blue dots) and the scattering lodging plots (red dots). We removed the lodging cultivars from model M1 and achieved an  $R^2$  of 0.88 compared to 0.81 for the relationship between dry biomass and  $PH_{CSM}$ . Similarly, for model validation,  $R^2$  increases from 0.60 to 0.64. This observation can explain the big differences between M3a and M3b, where the dataset was divided into old and new cultivars. Therefore, the best performing model, M3b, for fresh biomass is possibly influenced by the lodging effect.

**Figure 6.** Scatter plot for dry biomass *versus* CSM<sub>PH</sub>: lodging and non-lodging plots; n = 216.



Comparable results from UAV-based imaging are currently limited to the study by Grenzdörffer and Zacharias [43]. They found relationships of 0.6 and 0.76 between PH and yield in a grassland experiment. Most other studies focus on terrestrial laser scanning (TLS). Tilly *et al.* [24] estimated biomass with an  $R^2$  of 0.90 in a comparison between a field experiment and a farmer's field for paddy rice. In the study by Lumme *et al.* [27], a comparison of PH and estimated grain yield in barley, oat and wheat using a laser scanner mounted on a rack led to an  $R^2$  between 0.88 and 0.95. The results indicate that TLS yields higher accuracies in biomass estimation. However, the number of samples was slightly lower in the study by Tilly *et al.* [24] ( $n = 72$ ,  $n = 90$ ) obtained in a shorter observation period (21 June–19 July 2011) with only three measurements and only three cultivars, as opposed to 18 in this study. Lumme *et al.* [27] used three types of crops with five treatments ( $n = 15$ ) in six scans during the growing period. Furthermore, no lodging was reported for the comparative studies. Lodging and differences in plant development of the cultivars clearly influence biomass and PH. The results presented here need to be evaluated for field scale studies of multiple years to verify transferability. Several factors, such as water supply and temperature, soil type and status, the type of crop and the phenology, which are commonly considered in crop growth models [45,46], are not investigated here.

Both methods, the UAV-based CSM and the TLS-based CSM, produce highly detailed point clouds. Comparisons of TLS *versus* the UAV-based SfM approach show that competitive results can be achieved for excavation sites [47], dike inspection (SE 0.022–0.04 m) [48] and landslides (RMSE 0.31 m) [49], although the point density is considerably lower for the UAV-based approach. On the other hand, Höfle [50] suggests that occlusion effects of TLS are possibly avoided in the UAV approach. Data collected with UAVs might be less accurate, but UAVs offer the advantage of a fast, inexpensive and highly-flexible data collection method that can easily cover larger areas. Data acquisition of 1 ha takes about 2 h with TLS and 20 min with a UAV, assuming that the allowed time for ground control measurement and data analysis is equal. Purchasing a suitable laser scanner costs about 40,000 €, while a low-cost UAV-system can be bought from 4000 €, including an RGB sensor (Mk-Oktokopter, including autopilot (1500 €), GPS (300 €), battery (200 € each), remote control (MX-20 HoTT; 450 €), gimbal (MK HiSight SLR2; 450 €), sensor (Panasonic Lumic DMC GX1; 460 €) and lens (Panasonic Lumix G F1, 7/20 mm; 365 €) = 3725 €. Since autopilots and automated

take-off and landing mechanisms make data acquisition with a UAV feasible without intensive training, they will become directly applicable for a farmer or non-professional service providers [51] in the future.

In this study, uncertainties occur both in PH modelling and biomass modeling. The main constraint of the dataset are the lodging cultivars. Lodging causes a lower average PH than expected (Figure 6) and, thus, weakens the relationship between biomass and PH (*i.e.*,  $R^2 = 0.61$  compared to 0.64 for dry biomass M1). In addition, it appears from Figure 4 that scattering increases after PH reaches 0.5 m. This height is reached at the heading stage (Table 1). The standard error of  $PH_{CSM}$  varies between 0.007 and 0.019 m across growth stages and does show an increasing trend. Thus, a reason for the increased scattering is the higher SE in obtained destructively measured biomass. The SE doubles from 0.025 to 0.053 kg/m<sup>2</sup> when it reaches the heading stage. Therefore, it seems that growth stages influence the prediction accuracy due to increasing spatial variability. Generally, the robustness of the method must be further investigated, as we only used data from a single experiment in one year.

## 5. Conclusions and Outlook

In this study, we introduced a simple method for estimating biomass based on plant height derived from crop surface models. First, it was demonstrated that unmanned aerial vehicle (UAV)-based red, green, blue (RGB) optical images are highly suitable for deriving barley plant height (PH) from multi-temporal crop surface models (CSMs) with a super high resolution of 1 cm on the field scale. The PH can be modeled with a very high accuracy for different growth stages using UAV-based high resolution images ( $R^2 = 0.92$ ). The CSMs cover more details than point-wise ground measurements, where a lower mean PH per plot is obtained.

In the second step, a new method for estimating crop biomass based on PH was tested. Five linear models for estimating above-ground fresh and dry biomass were developed and tested through cross-validation. The models explain 61%–72% of the fresh and 39%–68% of the dry summer barley biomass variability in a controlled field experiment with 18 cultivars and two treatments throughout the vegetation period (May to July, 2013). The coefficients of determination ( $R^2 = 0.31$ –0.72) demonstrate that PH derived from UAV-based images is a suitable indicator for biomass. The model quality is limited through the lodging of four cultivars and increased biomass scattering after the booting stage. The results presented here need to be evaluated in multiple-year field-scale studies to ensure model robustness and transferability.

Improvements should be made in UAV-based image collection by using an inertial measurement unit (IMU) in combination with a global positioning system (GPS) on the MK-Oktokopter. The combination enables direct georeferencing of the images with cm accuracy. That way, the ground control points can be omitted, which speeds up both the data collection and the data processing. The first studies [52–55] show that this approach is close to operational use [29]. In a next step, the results from this study will be combined with (hyper-) spectral measurements for the calculation of vegetation indices. Vegetation indices can serve for the estimation of plant parameters, like chlorophyll or nitrogen concentration [18,56]. The first results from UAV-based hyperspectral full-frame imaging have been published [57,58]. Furthermore, vegetation indices in the visible domain have potential in crop monitoring [59,60]. Ultimately, the analysis of single growth stages should be performed.

## Acknowledgments

The authors acknowledge the funding of the CROP.SENSE.net project in the context of the Ziel 2-Programm North Rhine-Westphalia (NRW) 2007–2013 “Regionale Wettbewerbsfähigkeit und Beschäftigung (Europäischer Fonds für regionale Entwicklung (EFRE))” by the Ministry for Innovation, Science and Research (Ministerium für Innovation, Wissenschaft und Forschung (MIWF)) of the state North Rhine-Westphalia (NRW) and European Union Funds for regional development (EFRE) (005-1103-0018).

## Author Contributions

Simon Bennertz, Janis Broscheit and Silas Eichfuss collected the biomass samples, measured plant height in the field and processed the weight analysis in the laboratory. Simon Bennertz performed BBCH measurements. Juliane Bendig conducted the UAV campaigns, processed the CSMs, executed the biomass modelling and wrote the manuscript. Andreas Bolten assisted in the statistical analysis and the figure design. Georg Bareth provided expertise on biomass modelling and co-prepared the manuscript. Editorial contributions to the manuscript were made by Andreas Bolten and Georg Bareth.

## Conflicts of Interest

The authors declare no conflict of interest.

## References and Notes

1. Mulla, D.J. Twenty five years of remote sensing in precision agriculture: Key advances and remaining knowledge gaps. *Biosyst. Eng.* **2013**, *114*, 358–371.
2. Laudien, R.; Bareth, G. Multitemporal hyperspectral data analysis for regional detection of plant diseases by using a tractor- and an airborne-based spectrometer. *Photogramm. Fernerkund. Geoinf.* **2006**, *3*, 217–227.
3. Goynes, P.J.; Meinke, H.; Milroy, S.P.; Hammer, G.L.; Hare, J.M. Development and use of a barley crop simulation model to evaluate production management strategies in north-eastern Australia. *Crop. Pasture Sci.* **1996**, *47*, 997–1015.
4. Shanahan, J.F.; Schepers, J.S.; Francis, D.D.; Varvel, G.E.; Wilhelm, W.W.; Tringe, J.M.; Schlemmer, M.R.; Major, D.J. Use of remote-sensing imagery to estimate corn grain yield. *Agron. J.* **2001**, *93*, 583–589.
5. Adamchuk, V.I.; Ferguson, R.B.; Hergert, G.W. Soil heterogeneity and crop growth. In *Precision Crop Protection—The Challenge and Use of Heterogeneity*; Oerke, E.-C., Gerhards, R., Menz, G., Sikora, R.A., Eds.; Springer: Dordrecht, The Netherlands, 2010; pp. 3–16.
6. Thenkabail, P.S.; Smith, R.B.; De Pauw, E. Hyperspectral vegetation indices and their relationships with agricultural crop characteristics. *Remote Sens. Environ.* **2000**, *71*, 158–182.
7. Jensen, A.; Lorenzen, B.; Østergaard, H.S.; Hvelplund, E.K. Radiometric estimation of biomass and nitrogen content of barley grown at different nitrogen levels. *Int. J. Remote Sens.* **1990**, *11*, 1809–1820.

8. Chen, P.; Haboudane, D.; Tremblay, N.; Wang, J.; Vigneault, P.; Li, B. New spectral indicator assessing the efficiency of crop nitrogen treatment in corn and wheat. *Remote Sens. Environ.* **2010**, *114*, 1987–1997.
9. Lemaire, G.; Gastal, F. N uptake and distribution in plant canopies. In *Diagnosis of the Nitrogen Status in Crops*; Lemaire, D.G., Ed.; Springer: Berlin, Germany, 1997; pp. 3–43.
10. Lemaire, G.; Jeuffroy, M.-H.; Gastal, F. Diagnosis tool for plant and crop N status in vegetative stage. *Eur. J. Agron.* **2008**, *28*, 614–624.
11. Kumar, L.; Schmidt, K.; Dury, S.; Skidmore, A. Imaging spectrometry and vegetation science. In *Imaging Spectrometry*; Van der Meer, F.D., Jong, S.M.D., Eds.; Kluwer Academic Publishers: Dordrecht, The Netherlands, 2001; pp. 111–155.
12. Koppe, W.; Gnyp, M.L.; Hennig, S.D.; Li, F.; Miao, Y.; Chen, X.; Jia, L.; Bareth, G. Multi-temporal hyperspectral and radar remote sensing for estimating winter wheat biomass in the North China Plain. *Photogramm. Fernerkund. Geoinf.* **2012**, *3*, 281–298.
13. Migdall, S.; Bach, H.; Bobert, J.; Wehrhan, M.; Mauser, W. Inversion of a canopy reflectance model using hyperspectral imagery for monitoring wheat growth and estimating yield. *Precis. Agric.* **2009**, *10*, 508–524.
14. Yang, C.; Everitt, J.H.; Bradford, J.M. Yield estimation from hyperspectral imagery using spectral angle mapper (SAM). *Trans. ASABE* **2008**, *51*, 729–737.
15. Jang, G.-S.; Sudduth, K.A.; Hong, S.Y.; Kitchen, N.R.; Palm, H.L. Relating hyperspectral image bands and vegetation indices to corn and soybean yield. *Korean J. Remote Sens.* **2006**, *22*, 183–197.
16. Hoyos-Villegas, V.; Fritschi, F.B. Relationships among vegetation indices derived from aerial photographs and soybean growth and yield. *Crop Sci.* **2013**, *53*, 2631–2642.
17. Sakamoto, T.; Gitelson, A.A.; Nguy-Robertson, A.L.; Arkebauer, T.J.; Wardlow, B.D.; Suyker, A.E.; Verma, S.B.; Shibayama, M. An alternative method using digital cameras for continuous monitoring of crop status. *Agric. For. Meteorol.* **2012**, *154–155*, 113–126.
18. Gnyp, M.L.; Bareth, G.; Li, F.; Lenz-Wiedemann, V.I.S.; Koppe, W.; Miao, Y.; Hennig, S.D.; Jia, L.; Laudien, R.; Chen, X.; *et al.* Development and implementation of a multiscale biomass model using hyperspectral vegetation indices for winter wheat in the North China Plain. *Int. J. Appl. Earth Obs. Geoinf.* **2014**, *33*, 232–242.
19. Li, F.; Miao, Y.; Hennig, S.D.; Gnyp, M.L.; Chen, X.; Jia, L.; Bareth, G. Evaluating hyperspectral vegetation indices for estimating nitrogen concentration of winter wheat at different growth stages. *Precis. Agric.* **2010**, *11*, 335–357.
20. Lati, R.N.; Filin, S.; Eizenberg, H. Estimating plant growth parameters using an energy minimization-based stereovision model. *Comput. Electron. Agric.* **2013**, *98*, 260–271.
21. Bendig, J.; Bolten, A.; Bareth, G. UAV-based imaging for multi-temporal, very high resolution crop surface models to monitor crop growth variability. *Photogramm. Fernerkund. Geoinf.* **2013**, *6*, 551–562.
22. Hoffmeister, D.; Bolten, A.; Curdt, C.; Waldhoff, G.; Bareth, G. High-resolution Crop Surface Models (CSM) and Crop Volume Models (CVM) on field level by terrestrial laser scanning. *Proc. SPIE* **2010**, *7840*, doi:10.1117/12.872315.

23. Hoffmeister, D.; Waldhoff, G.; Curdt, C.; Tilly, N.; Bendig, J.; Bareth, G. Spatial variability detection of crop height in a single field by terrestrial laser scanning. In *Precision Agriculture'13*; Stafford, J.V., Ed.; Wageningen Academic Publishers: Lleida, Spain, 2013; pp. 267–274.
24. Tilly, N.; Hoffmeister, D.; Cao, Q.; Huang, S.; Lenz-Wiedemann, V.I.S.; Miao, Y.; Bareth, G. Multitemporal crop surface models: Accurate plant height measurement and biomass estimation with terrestrial laser scanning in paddy rice. *J. Appl. Remote Sens.* **2014**, *8*, 083671–083671.
25. Tilly, N.; Hoffmeister, D.; Liang, H.; Cao, Q.; Liu, Y.; Lenz-Wiedemann, V.; Miao, Y.; Bareth, G. Evaluation of terrestrial laser scanning for rice growth monitoring. *Int. Arch. Photogramm. Remote Sens. Spat. Inf. Sci.* **2012**, *XXXIX-B7*, 351–356.
26. Hoffmeister, D.; Curdt, C.; Tilly, N.; Bendig, J.; Bareth, G. 3D change detection of different sugar-beet types by multi-temporal terrestrial laser scanning. In Proceedings of 2011 International Symposium on Remote Sensing and GIS Methods for Change Detection and Spatio-Temporal Modelling (CDSM); Hong Kong, China, 15–16 December 2011; p. 5.
27. Lumme, J.; Karjalainen, M.; Kaartinen, H.; Kukko, A.; Hyypä, J.; Hyypä, H.; Jaakkola, A.; Kleemola, J. Terrestrial laser scanning of agricultural crops. *Int. Arch. Photogramm. Remote Sens. Spat. Inf. Sci.* **2008**, *37*, 563–566.
28. Ehlert, D.; Adamek, R.; Horn, H.-J. Laser rangefinder-based measuring of crop biomass under field conditions. *Precis. Agric.* **2009**, *10*, 395–408.
29. Colomina, I.; Molina, P. Unmanned aerial systems for photogrammetry and remote sensing: A review. *ISPRS J. Photogramm. Remote Sens.* **2014**, *92*, 79–97.
30. Zarco-Tejada, P.J. A new era in remote sensing of crops with unmanned robots. *Proc. SPIE* **2008**, *7480*, 2–4.
31. Jensen, T.; Apan, A.; Young, F.; Zeller, L. Detecting the attributes of a wheat crop using digital imagery acquired from a low-altitude platform. *Comput. Electron. Agric.* **2007**, *59*, 66–77.
32. Hunt, E.R.; Hively, W.D.; McCarty, G.W.; Daughtry, C.S.T.; Forrestal, P.J.; Kratochvil, R.J.; Carr, J.L.; Allen, N.F.; Fox-Rabinovitz, J.R.; Miller, C.D. NIR-green-blue high-resolution digital images for assessment of winter cover crop biomass. *GISci. Remote Sens.* **2011**, *48*, 86–98.
33. Agüera, F.; Carvajal, F.; Pérez, M. Measuring sun-flower nitrogen status from an unmanned aerial vehicle-based system and an on the ground device. *Int. Arch. Photogramm. Remote Sens. Spat. Inf. Sci.* **2011**, *38*, 33–37.
34. Berni, J.A.J.; Zarco-Tejada, P.J.; Suárez, L.; González-Dugo, V.; Fereres, E. Remote sensing of vegetation from UAV platforms using lightweight multispectral and thermal imaging sensors. *Int. Arch. Photogramm. Remote Sens. Spat. Inf. Sci.* **2009**, *38*, 6.
35. Baluja, J. Assessment of vineyard water status variability by thermal and multispectral imagery using an Unmanned Aerial Vehicle (UAV). *Irrig. Sci.* **2012**, *6*, 511–522.
36. Turner, D.; Lucieer, A.; Malenovský, Z.; King, D.; Robinson, S. Spatial co-registration of ultra-high resolution visible, multispectral and thermal images acquired with a micro-UAV over Antarctic Moss Beds. *Remote Sens.* **2014**, *6*, 4003–4024.
37. Verhoeven, G. Taking computer vision aloft—Archaeological three-dimensional reconstructions from aerial photographs with photostan. *Archaeol. Prospect.* **2011**, *18*, 67–73.

38. Turner, D.; Lucieer, A.; Watson, C. An automated technique for generating georectified mosaics from ultra-high resolution unmanned aerial vehicle (UAV) imagery, based on structure from motion (SfM) point clouds. *Remote Sens.* **2012**, *4*, 1392–1410.
39. Lucieer, A.; Turner, D.; King, D.H.; Robinson, S.A. Using an Unmanned Aerial Vehicle (UAV) to capture micro-topography of Antarctic moss beds. *Int. J. Appl. Earth Obs. Geoinf.* **2014**, *27*, 53–62.
40. Baiocchi, V.; Dominici, D.; Elaiopoulos, M.; Massimi, V.; Mormile, M.; Rosciano, E. UAV flight plan software: first implementation of UP23d. In Proceedings of 2013 EARSeL Symposium Towards Horizon 2020: Earth Observation and Social Perspectives, Matera, Italy, 3–6 June 2013; pp. 829–841.
41. Ehlert, D.; Horn, H.-J.; Adamek, R. Measuring crop biomass density by laser triangulation. *Comput. Electron. Agric.* **2008**, *61*, 117–125.
42. Busemeyer, L.; Mentrup, D.; Möller, K.; Wunder, E.; Alheit, K.; Hahn, V.; Maurer, H.P.; Reif, J.C.; Würschum, T.; Müller, J.; *et al.* Breedvision—A multi-sensor platform for non-destructive field-based phenotyping in plant breeding. *Sensors* **2013**, *13*, 2830–2847.
43. Grenzdörffer, G.; Zacharias, P. Bestandeshöhenermittlung landwirtschaftlicher Kulturen aus UAS-Punktwolken. *DGPF Tagungsband* **2014**, *23*, 1–8.
44. Scotford, I.M.; Miller, P.C.H. Combination of spectral reflectance and ultrasonic sensing to monitor the growth of winter wheat. *Biosyst. Eng.* **2004**, *87*, 27–38.
45. Clevers, J.P.G.W.; Jongschaap, R. Imaging spectrometry for agricultural applications. In *Imaging Spectrometry*, Van der Meer, F.D., Jong, S.M.D., Eds.; Kluwer Academic Publishers: Dordrecht, The Netherlands, 2001; pp. 157–199.
46. Confalonieri, R.; Bregaglio, S.; Rosenmund, A.S.; Acutis, M.; Savin, I. A model for simulating the height of rice plants. *Eur. J. Agron.* **2011**, *34*, 20–25.
47. Doneus, M.; Verhoeven, G.; Fera, M.; Briese, C.; Kucera, M.; Neubauer, W. From deposit to point cloud: a study of low-cost computer vision approaches for the straightforward documentation of archaeological excavations. In Proceedings of 2011 International CIPA Symposium, Prague, Czech Republic, 12–16 September 2011; pp. 81–88.
48. Naumann, M.; Bill, R.; Niemeyer, F.; Nitschke, E. Deformation analysis of dikes using Unmanned Aerial Systems (UAS). In Proceedings of the South Baltic Conference on Dredged Materials in Dike Construction, Rostock, Germany, 10–12 April 2014; pp. 119–126.
49. Niethammer, U.; James, M.R.; Rothmund, S.; Travelletti, J.; Joswig, M. UAV-based remote sensing of the Super-Sauze landslide: Evaluation and results. *Eng. Geol.* **2012**, *128*, 2–11.
50. Höfle, B. Radiometric correction of terrestrial LiDAR point cloud data for individual maize plant detection. *IEEE Geosci. Remote Sens. Lett.* **2014**, *1*, 94–98.
51. Swain, K.C.; Thomson, S.J.; Jayasuriya, H.P.W. Adoption of an unmanned helicopter for low-altitude remote sensing to estimate yield and total biomass of a rice crop. *Trans. ASAE* **2010**, *53*, 21–27.
52. Eling, C.; Klingbeil, L.; Wieland, M.; Kuhlmann, H. A precise position and attitude determination system for lightweight unmanned aerial vehicles. *Int. Arch. Photogramm. Remote Sens. Spat. Inf. Sci.* **2013**, *XL-1/W2*, 113–118.
53. Turner, D.; Lucieer, A.; Wallace, L. Direct georeferencing of ultrahigh-resolution UAV imagery. *IEEE Trans. Geosci. Remote Sens.* **2014**, *52*, 2738–2745.

54. Pfeifer, N.; Glira, P.; Briese, C. Direct georeferencing with on board navigation components of light weight UAV platforms. *Int. Arch. Photogramm. Remote Sens. Spat. Inf. Sci.* **2012**, *XXXIX-B7*, 487–492.
55. Eling, C.; Klingbeil, L.; Wieland, M.; Kuhlmann, H. Direct georeferencing of micro aerial vehicles—System design, system calibration and first evaluation tests. *Photogramm. Fernerkund. Geoinf.* **2014**, *4*, 227–237.
56. Yu, K.; Lenz-Wiedemann, V.; Leufen, G.; Hunsche, M.; Noga, G.; Chen, X.; Bareth, G. Assessing hyperspectral vegetation indices for estimating leaf chlorophyll concentration of summer barley. *ISPRS Ann. Photogramm. Remote Sens. Spat. Inf. Sci.* **2012**, *I-7*, 89–94.
57. Bareth, G.; Bendig, J.; Aasen, H.; Gnyp, M.L.; Bolten, A.; Jung, A.; Michels, R.; Soukkamäki, J. Low-weight and UAV-based hyperspectral full-frame cameras for monitoring crops: Spectral comparison with portable spectroradiometer measurements. *Photogramm. Fernerkund. Geoinf.* **2015**, in press.
58. Honkavaara, E.; Saari, H.; Kaivosoja, J.; Pölönen, I.; Hakala, T.; Litkey, P.; Mäkynen, J.; Pesonen, L. Processing and assessment of spectrometric, stereoscopic imagery collected using a lightweight UAV spectral camera for precision agriculture. *Remote Sens.* **2013**, *5*, 5006–5039.
59. Hunt, E.R., Jr.; Cavigelli, M.; Daughtry, C.S.T.; McMurtrey, J.E., III; Walthall, C.L. Evaluation of digital photography from model aircraft for remote sensing of crop biomass and nitrogen status. *Precis. Agric.* **2005**, *6*, 359–378.
60. Hunt, E.R., Jr.; Doraiswamy, P.C.; McMurtrey, J.E.; Daughtry, C.S.T.; Perry, E.M.; Akhmedov, B. A visible band index for remote sensing leaf chlorophyll content at the canopy scale. *Int. J. Appl. Earth Obs. Geoinf.* **2013**, *21*, 103–112.

© 2014 by the authors; licensee MDPI, Basel, Switzerland. This article is an open access article distributed under the terms and conditions of the Creative Commons Attribution license (<http://creativecommons.org/licenses/by/4.0/>).